Development 133, 3827-3836 (2006) doi:10.1242/dev.02559

Knockdown of $Na_v1.6a$ Na^+ channels affects zebrafish motoneuron development

Ricardo H. Pineda[1,*], Kurt R. Svoboda[1,2,*], Melissa A. Wright[1,*], Alison D. Taylor[1,*], Alicia E. Novak[1], Joshua T. Gamse[3], Judith S. Eisen[4] and Angeles B. Ribera[1,†]

In addition to rapid signaling, electrical activity provides important cues to developing neurons. Electrical activity relies on the function of several different types of voltage-gated ion channels. Whereas voltage-gated Ca^{2+} channel activity regulates several aspects of neuronal differentiation, much less is known about developmental roles of voltage-gated Na^+ channels, essential mediators of electrical signaling. Here, we focus on the zebrafish Na^+ channel isotype, $Na_v1.6a$, which is encoded by the *scn8a* gene. A restricted set of spinal neurons, including dorsal sensory Rohon-Beard cells, two motoneuron subtypes with different axonal trajectories, express *scn8a* during embryonic development. CaP, an early born primary motoneuron subtype with ventrally projecting axons expresses *scn8a*, as does a class of secondary motoneurons with axons that project dorsally. To test for developmental roles of *scn8a*, we knocked down $Na_v1.6a$ protein using antisense morpholinos. Na^+ channel protein and current amplitudes were reduced in neurons that express *scn8a*. Furthermore, $Na_v1.6a$ knockdown altered axonal morphologies of some but not all motoneurons. Dorsally projecting secondary motoneurons express *scn8a* and displayed delayed axonal outgrowth. By contrast, CaP axons developed normally, despite expression of the gene. Surprisingly, ventrally projecting secondary motoneurons, a population in which *scn8a* was not detected, displayed aberrant axonal morphologies. Mosaic analysis indicated that effects on ventrally projecting secondary motoneurons were non cell-autonomous. Thus, voltage-gated Na^+ channels play cell-autonomous and non cell-autonomous roles during neuronal development.

KEY WORDS: Motoneuron, Na^+ channel, Axonal morphology, Zebrafish embryo

INTRODUCTION

Motoneuron axons project out of the central nervous system into the periphery and select among several potential muscle targets. Several activity-independent mechanisms influence pathfinding, while axons navigate through the periphery en route to their final muscle targets (for reviews, see Lewis and Eisen, 2003; Schneider and Granato, 2003). Once targets are contacted, both activity-dependent and -independent processes contribute to synapse formation, stabilization and maintenance (for a review, see Sanes and Lichtman, 2001). These findings have led to the traditional view that activity-independent mechanisms guide axons prior to synapse formation.

Interestingly, outgrowing axons often form synapses at intermediate points before they reach their final targets (Lefebvre et al., 2004). Further, spinal cord neurons exhibit spontaneous activity while their axons are actively extending processes (for a review, see Spitzer et al., 2004). Moreover, disruption of normal patterns of spontaneous activity alters neurotransmitter phenotypes, as well as motoneuron axonal pathfinding (Borodinsky et al., 2004; Hanson and Landmesser, 2004). Thus, activity-dependent mechanisms influence pathfinding before axons reach their final targets.

The role of activity is usually considered from the perspective of the synapse, despite the fact that embryonic neurons are electrically excitable prior to synapse formation (Spitzer et al., 2004). In addition, intrinsic excitability of embryonic neurons influences several key aspects of differentiation (Gu and Spitzer, 1995; Watt et al., 2000). However, little is known about how motoneuron intrinsic excitability influences axon outgrowth, especially while their processes navigate through the periphery (but see Ming et al., 2001).

A key determinant of neuronal excitability is the voltage-gated Na^+ channel. A spontaneously occurring mouse mutant, *med* (*motor endplate disease*), displays a paralytic phenotype (Duchen, 1970; Duchen and Stefani, 1971). The *med* mutation leads to inactivation of the *Scn8a* Na^+ channel α-subunit gene that encodes the mammalian $Na_v1.6$ protein (Burgess et al., 1995). The orthologous zebrafish gene, *scn8a*, encodes the zebrafish $Na_v1.6a$ protein and is expressed early in the developing spinal cord (Tsai et al., 2001; Novak et al., 2006a; Novak et al., 2006b). Here, we test whether $Na_v1.6a$ regulates development of embryonic spinal neurons. $Na_v1.6a$ knockdown alters development of several, but not all, *scn8a*-expressing neurons. Moreover, neuronal subtypes that do not express *scn8a* also display developmental defects, revealing non cell-autonomous roles of ion channels during neuronal development.

MATERIALS AND METHODS

Zebrafish lines and maintenance

Zebrafish were housed at 28°C in the Aquatics Facility maintained by the UCDHSC Center for Animal Laboratory Care/Center for Comparative Medicine. We used three different wild-type strains (Tü, AB and PS; the latter are fish from a local pet store) and the following transgenic lines: Tg(flh:GFP), Tg(gata2:GFP) and Tg(isl1:GFP) (kindly provided by M. Halpern, S. Lin and S. Higashijima) (Higashijima et al., 2000; Meng et al., 1997; Gamse et al., 2003). Twenty-two to 24 hours post fertilization (hpf) embryos were manually dechorionated and transferred to embryo medium [EM; Westerfield (Westerfield, 1995)] containing 0.002% 1-phenyl-2-thiourea, to inhibit pigment formation.

[1]Department of Physiology and Biophysics, 8307 University of Colorado Denver and Health Sciences Center, Aurora, CO 80045, USA. [2]Department of Biological Sciences, Louisiana State University, Baton Rouge, LA 70803, USA. [3]Department of Biological Sciences, Vanderbilt University, Nashville, TN 37232, USA. [4]Institute of Neuroscience, 1254 University of Oregon, Eugene, OR 97403, USA.

*These authors contributed equally to this work
†Author for correspondence (e-mail: angie.ribera@uchsc.edu)

Accepted 2 August 2006

Embryos were staged on the basis of external morphological criteria and age is indicated by standard convention in terms of hours or days post fertilization (hpf or dpf) (Kimmel et al., 1995). Developmental landmarks that aided staging included somite number, head-trunk angle, yolk sac size and position, and pectoral fin buds.

Morpholino injections

Morpholino antisense oligonucleotides (MOs) were synthesized by Gene Tools (Philomath, Oregon). The $Na_v1.6a$ MO (1.6MO) targeted the predicted translation start methionine of $Na_v1.6a$ and had 25 residues with the following sequence: 5′GGGTGCAGCCATGTTTTCATCCTGC-3′. Two other 1.6MOs, with sequences either slightly downstream or upstream, were also synthesized. A fourth MO that targeted the splice junction between exons 3 and 4 was also synthesized. Similar results were obtained with the four different (three translation-blocking and one splice-blocking) 1.6MOs, and the results were pooled. 1.6MO-injected embryos are referred to as morphants. Two control MOs (ConMOs), differing from a translation blocking or splice blocking MO by five base mismatches, were synthesized. ConMO-injected embryos served as controls. MOs were injected into the yolk at one- to two-cell at concentrations ranging between 2.5 and 4 ng/nl in 1% Fast Green or rhodamine-conjugated dextran.

Reverse transcription-polymerase chain reaction (RT-PCR)

RNA was collected from whole 24, 48 or 72 hpf embryos that had been injected with either the splice blocking MO or its control MO using the TRIzol Reagent (Invitrogen, Carlsbad, CA). cDNA synthesis was performed using oligo dT (GIBCO-BRL, Gaithersburg, MD) and Superscript II reverse transcriptase (RT; GIBCO-BRL). The PCR conditions were 5 minutes at 95°C; five cycles at 95°C for 1 minute, 50°C for 30 seconds, 72°C for 30 seconds; five cycles at 95°C for 1 minute, 51°C for 30 seconds, 72°C for 30 seconds; 25 cycles at 95°C for 1 minute, 52°C for 30 seconds, 72°C for 30 seconds; followed by 72°C for 7 minutes. The negative control tested for amplification of genomic DNA and consisted of preparing an RT reaction tube but omitting the RT enzyme. PCR products were gel purified and cloned (PCR-Script Cloning Kit, Stratagene, La Jolla, CA). DNA sequencing confirmed their identity.

In situ hybridization

Procedures were as described in Novak and Ribera (Novak and Ribera, 2003). For double in situ hybridization, the second probe was synthesized in the presence of fluorescein-labeled nucleotide precursors (Roche); the probe was detected with an anti-fluorescein antibody coupled to horseradish peroxidase, allowing formation of a green fluorescent reaction product using tyramide based signal amplification (Perkin Elmer, Boston, MA).

Immunocytochemistry

Procedures were as described previously (Svoboda et al., 2001). We used the primary antibodies listed in Table 1. The anti-Islet 39.4D5, 3A10, SV-2, zn-8, zn-12 and znp-1 mouse monoclonals were developed by Drs T. Jessell (39.4D5. 3A10), J. Dodd (3A10), K. Buckley (SV-2) and B. Trevarrow (zn-8, zn-12, znp-1), and were obtained from the Developmental Studies Hybridoma Bank developed under the auspices of the NICHD and maintained by The University of Iowa, Department of Biological Sciences, Iowa City, IA 52242. Secondary antibody was applied during a subsequent overnight incubation at 4°C (1:1000; anti-rabbit or anti-mouse conjugated to either Alexa 548 or Alexa 488; Molecular Probes). Embryos were squash-mounted on glass slides in 20 μl Prolong AntiFade Reagent (Molecular Probes).

Dye-labeling primary motoneurons

Primary motoneurons (PMNs) were labeled as described previously (Eisen et al., 1986) with the following minor modifications. Embryos were injected at 19-21 hpf and fixed 1-3 hours later. Whole-mount preparations were incubated with rabbit anti-fluorescein antibodies (Molecular Probes) and the SV-2 monoclonal antibody (Table 1). Secondary antibody application and subsequent processing was as described above.

Mosaic embryos

Mosaic embryos were created by injection of single cells in 2 to 3 hpf wild-type of Tg(gata2:GFP) embryos with solution containing 0.3 mM MO and lineage tracer (1-3% lysinated-rhodamine- or fluorescein-labeled dextran; 10,000 M_r). Embryos were fixed at 72 hpf and processed for dextran and GFP or zn-8 immunoreactivities (see below).

Visualization of RNA in situ hybridization signals or antibody labeling

Embryos were viewed on either a Nikon Eclipse TE2000 inverted scope at 40× or a Zeiss Pascal Confocal microscope at 10, 40 or 63×. Images were acquired digitally and processed using Adobe Photoshop Software (Mountain View, CA). For confocal imaging, the pinhole was set to one Airy unit. Rhodamine/Alexa-568 and Fluorescein/Alexa 488 were visualized using separate channels. *Z*-stacks were collected at 1-1.5 μm intervals; data are presented as single sections unless indicated otherwise. Because embryos were squash-mounted, it was possible to view motor nerves from both sides of an embryo in a single section (e.g. Figs 5, 7). To determine the percent of pixels in a field that showed signals above threshold for both channels, we used the colocalization algorithm of the Zeiss Pascal LSM software.

Electrophysiology

Embryos dissections and nucleated patch recordings were performed as described previously (Ribera and Nüsslein-Volhard, 1998; Pineda et al., 2005). We used nucleated patches to avoid space clamp problems. The recording solution consisted of: 127 mM NaCl, 20 mM TEA-Cl, 3 mM KCl, 10 mM $CoCl_2$, and 10 mM HEPES (pH 7.2). Electrodes had resistances of 2-3 MΩ when filled with pipet solution [125 mM CsCl, 12 mM NaCl, 10 mM EGTA and 10 mM HEPES (pH 7.2)]. Recordings were made using an Axopatch 200B Amplifier (Axon Instruments) and were continued when the following criteria were met online: (1) input resistances greater than 1GΩ; and (2) mono-exponential decay of the whole cell capacitance transient. The pCLAMP9 and Origin programs (Axon Instruments) were used to analyze data.

Table 1. Primary antibody information

Antibody	Source	Concentration	Epitope	References
3A10	DSHB*	1:10	Several neuronal antigens, including synapsin	Hatta (1992), Harada et al. (1999)
Anti-acetylated tubulin	Sigma	1:1000	Acetylated tubulin	Svoboda et al. (2001)
Anti-GFP	Molecular Probes	1:750	GFP	
Anti-Hu (16A11)	Molecular Probes	1:1000	Hu (RNA-binding protein)	Marusich et al. (1994), Henion et al. (1996)
Anti-Isl (39.4D5)	DSHB*	1:100	Islet1 and Islet2 (transcription factors)	
Anti-Na^+ channel (Pan)	Sigma	1:500	All voltage-gated Na^+ channels	
Anti-SV2	DSHB*	1:100	SV2 (synaptic vesicle marker)	Panzer et al. (2005)
Zn-8/neurolin	DSHB*	1:200	Secondary motoneuron axons	Fashena and Westerfield (1999)
Zn-12/HNK-1	DSHB*	1:500	Neuronal axons	Metcalfe et al. (1990)
Znp-1	DSHB*	1:100	Motoneuron axons	Trevarrow et al. (1990)

*Developmental Studies Hybridoma Bank.

RESULTS

Early expression of *scn8a* in the embryonic spinal cord

To identify the role that the *scn8a* gene plays during development of the embryonic vertebrate nervous system, we first determined its mRNA expression pattern in the zebrafish embryo. Between 24 and 72 hpf, *scn8a* transcripts were detected in several populations of spinal neurons (Figs 1, 2). The most dorsal *scn8a*$^+$ neurons also expressed the RNA-binding protein Hu, identifying them as mechanosensory Rohon-Beard (RB) cells (Fig. 1A-C) (Marusich et al., 1994; Henion et al., 1996).

Ventral spinal neurons also contained *scn8a* transcripts (Fig. 1D-G). The position of ventral *scn8a*$^+$ cells suggested that some might be motoneurons. Primary motoneurons (PMNs) are born during gastrulation, whereas secondary motoneurons (SMNs) arise from later rounds of neurogenesis (Beattie et al., 1997). To identify the PMN subtype(s) that expressed *scn8a*, we used specific markers of PMN subtypes and the Tg(flh:GFP) transgenic line (Gamse et al., 2003). By 24 hpf, PMN subtypes can be distinguished on the basis of their axonal trajectories (for a review, see Lewis and Eisen, 2003): RoP axons innervate the region around the horizontal myoseptum. MiPs have axons that project dorsally, whereas CaP axons innervate ventral trunk muscle. Tg(flh:GFP) transgenic embryos displayed GFP in CaPs (arrowheads), identified on the basis of ventrally projecting axons (arrows) (Fig. 1D) (Gamse et al., 2003). The Islet (Isl) antibody recognizes Islet1 as well as Islet2 transcription factors found in RB cells (asterisks) and PMNs (arrowheads) (Fig. 1D). However, MiPs and CaPs differentially express islet transcription factor genes, and *isl1* mRNA localizes to MiPs, whereas *isl2* transcripts are present in CaPs (Appel et al., 1995; Inoue et al., 1994; Tokumoto et al., 1995). Consistent with this, GFP$^-$ neurons in the Tg(flh:GFP) line expressed *isl1* mRNA, a marker of MiPs (Fig. 1E, carats). Thus, CaPs are the GFP$^+$ PMNs in Tg(flh:GFP) embryos. Furthermore, in situ hybridization revealed that *scn8a* transcripts localized to the GFP$^+$ CaPs (Fig. 1F). Consistent with this, double in situ hybridization studies indicated that CaPs, identified on the basis of *isl2* mRNA (Fig. 1G, green), also expressed *scn8a* (Fig. 1G, red). Thus, CaPs are the PMN subset that expressed *scn8a*.

We tested whether SMNs expressed *scn8a* by using transgenic lines that have different populations of SMNs labeled by GFP. In the Tg(isl1:GFP) transgenic line, GFP is present in SMNs that project dorsally, similarly to MiPs (Higashijima et al., 2000). *scn8a* mRNA was detected in GFP$^+$ SMNs of at both 36 and 72 hpf (Fig. 2A,C). Interestingly, despite expression of *scn8a* in CaPs, ventrally projecting SMNs did not express the gene. In Tg(gata2:GFP) embryos, GFP identifies SMNs with axons that project ventrally, similar to CaPs (Meng et al., 1997). However, these GFP$^+$ SMNs did not display *scn8a* at either 36 or 72 hpf (Fig. 2B,D). In sum, only a subset of PMNs and SMNs expressed *scn8a*. Moreover, the PMN and SMN populations that expressed *scn8a* differed with respect to axonal trajectories.

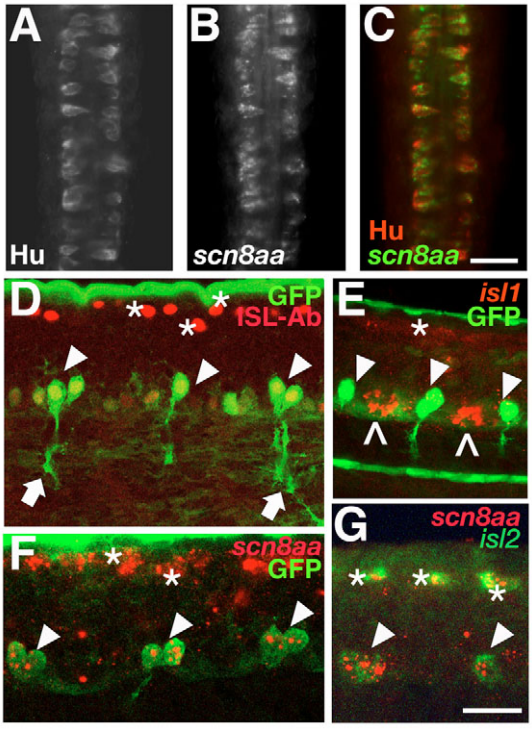

Fig. 1. Two primary spinal neuron types, RB cells and CaPs, expressed *scn8a*. (**A**) Hu immunoreactivity revealed RB somata in a 48 hpf embryo. (**B**) In situ hybridization indicated that dorsal spinal cord neurons contained *scn8a* transcripts. (**C**) Dual examination of Hu immunoreactivity and *scn8a* mRNA identified RB cells as the dorsal neurons that express *scn8a*. (**D**) GFP$^+$ neurons (arrowheads) in Tg(flh:GFP) embryos projected their axons (arrows) to ventral muscle, indicating that they were CaPs. In addition, GFP$^+$ neurons were ISL$^+$ (arrowheads, yellow nuclei), as were RB cells (asterisks). In two of the three hemisegments shown, VaPs were present with adjacent CaPs. VaPs are essentially duplicated CaPs that do not extend their axons as far ventrally, because of competition (Eisen, 1992; Eisen and Melancon, 2001). (**E**) GFP$^+$ neurons (arrowheads) in Tg(flh:GFP) embryos did not express *isl1* mRNA (carats), a marker of MiP. In the middle hemisegment, both CaP and VaP were present. (**F**) GFP$^+$ CaPs (arrowheads) in Tg(flh:GFP) embryos expressed *scn8a*, as did dorsal RB cells (asterisks). (**G**) Double in situ hybridization for *isl2*, a marker of CaP, and for *scn8a* revealed that both CaPs (arrowheads) as well as RB cells (asterisks) expressed *scn8a*. (A-C) Dorsal views, (D-G) lateral views, anterior is towards the left and dorsal is upwards. Scale bars: in C, 30 μm for A-C; in G, 30 μm in D-F; 15 μm in G.

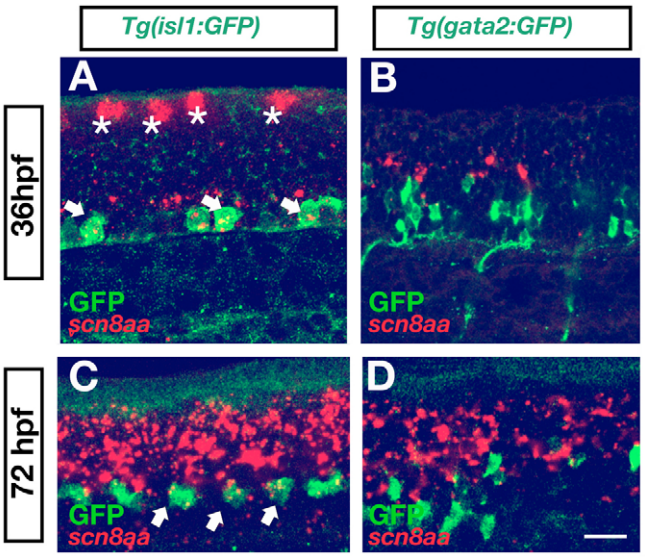

Fig. 2. Dorsally projecting, but not ventrally projecting, SMNs expressed *scn8a* mRNA. GFP$^+$ dorsally projecting SMNs in Tg(isl1:GFP) embryos expressed *scn8a* mRNA at 36 (**A**) and 72 (**C**) hpf (arrows). Asterisk in A indicates RB cells. (B) By contrast, ventrally projecting SMNs [GFP$^+$ in Tg(gata2:GFP) embryos] did not express *scn8a* at either 36 (**B**) or 72 (**D**) hpf. Scale bar: 25 μm in A,C; 40 μm in B,D.

Injection of 1.6MO resulted in reduction of Na^+ channel protein and current amplitude

To reveal the function of the *scn8a* gene, we used antisense MOs to inhibit splicing or translation. The translation blocking MOs were previously shown to work in a specific and dose-dependent manner (Pineda et al., 2005). The efficacy of the splice blocking MO was tested by RT-PCR. The splice blocking MO targeted the junction between the third and fourth exons. In RNA extracted from 24, 48 and 72 hpf morphant embryos, the 96 bp intron between these exons was retained until at least 72 hpf (Fig. 3A). Direct sequencing of the PCR product confirmed that the 96 bp intron had been retained, resulting in a premature STOP codon (results not shown). By contrast, in control-injected embryos, normal splicing occurred.

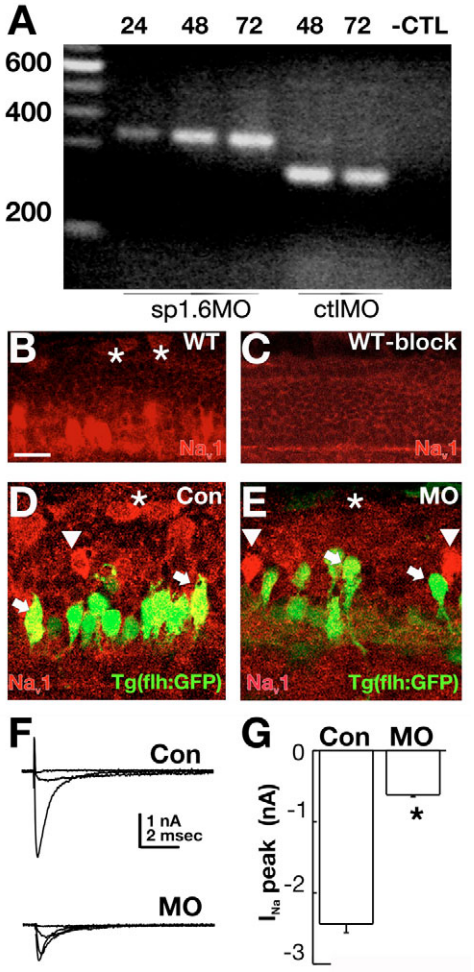

Fig. 3. Injection of 1.6MO blocked splicing and abolished Na^+ channel immunoreactivity and current in spinal cord neurons that expressed *scn8a* mRNA. (**A**) In RNA isolated from embryos injected with the splice blocking MO, excision of the 96 bp intron between exons 3 and 4 did not occur. This was true at 24, 48 and 72 hpf. By contrast, embryos injected with a control splice MO displayed normal splicing at this junction. (**B-E**) Na^+ channel immunoreactivity in control and morphant embryos. (B) A pan-specific Na^+ channel antibody revealed immunoreactivity in several classes of spinal cord neurons in 48 hpf wild-type embryos. RB cells (asterisks) and ventral neurons were brightly labeled. (C) Preincubation of the antibody with peptide blocked immunodetection of Na^+ channels. (D) GFP^+ ventral neurons (arrowhead, arrows) in Tg(flh:GFP) embryos displayed Na^+ channel immunoreactivity. (E) The 1.6MO reduced Na^+ channel immunoreactivity in some (arrows, asterisks) but not all (arrowheads) spinal neurons. Scale bar: 10 μm. (**F**) Na^+ currents recorded from RB cells of control embryos had larger amplitudes than those recorded from 1.6MO morphants. (**G**) Peak Na^+ current amplitude was significantly reduced in RB cells of 1.6MO morphants (n=6) versus control (n=6) embryos (*$P \leqslant 0.001$).

The efficacy of the 1.6MO in reducing Na^+ channel protein levels was assessed immunocytochemically and electrophysiologically. We performed immunocytochemical analyses with an antibody that recognizes all known (Pan) Na^+ channel isoforms (anti-Na^+ channel Pan). Wild type 48 hpf embryos displayed pan-Na channel immunoreactivity in several spinal cord neurons (Fig. 3B). Preincubation with the immunogenic peptide blocked immunoreactivity, indicating that the signal reflected specific detection of Na^+ channels (Fig. 3C). Following injection of the ConMO, 48 hpf embryos continued to display widespread Na^+ channel immunoreactivity in RB cells and motoneurons (Fig. 3E). By contrast, injection of the 1.6MO led to a dramatic reduction of Na^+ channel protein in some but not all spinal neurons (Fig. 3E). For example, labeling of RB cells by the antibody was suppressed (Fig. 3E, asterisks). In addition, fewer ventral cells were immunopositive (Fig. 3E, arrows). Importantly, several spinal neurons continued to display strong Na^+ channel immunoreactivity (Fig. 4E, arrowheads). These results indicated that injection of the 1.6MO led to Na^+ channel protein knockdown in some but not all neurons in the spinal cord, consistent with the restricted expression of *scn8a* (Figs 1, 2).

In addition to examining protein expression, we assessed the effects of the 1.6 and ConMOs by recording voltage-gated Na^+ current. Injection of the ConMO had no effect on voltage-gated Na^+ current (I_{Na}) recorded from RB cells of 48 hpf control embryos (Fig. 3F). By contrast, RB cells in 48 hpf morphants displayed either no I_{Na} or one of dramatically reduced amplitude (Fig. 3F,G). On average, peak I_{Na} amplitude was 25% that of control (Fig. 3G). The electrophysiological data were consistent with the previously described touch-insensitive behavioral phenotype of 1.6MO morphants (Pineda et al., 2005). We also found that 1.6MO morphants became increasingly more immotile with time and displayed little spontaneous swimming after 72 hpf.

In summary, two different measures of Na^+ channel protein, immunoreactivity and current, were reduced in *scn8a* expressing neurons following injection of 1.6, but not control, MO. These results indicated that 1.6MO injection was an effective strategy for $Na_v1.6a$ knockdown in the developing embryo.

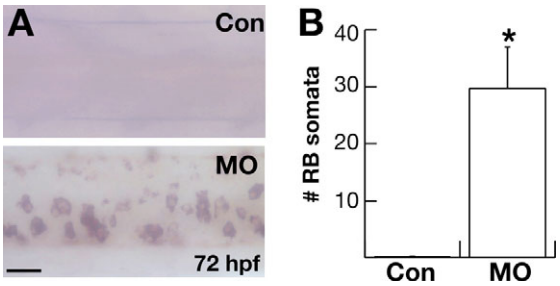

Fig. 4. RB cells survived longer in 1.6MO morphants embryos. (**A**) Injection of the 1.6MO prolonged RB survival in 72 hpf 1.6MO morphants embryos. RB cells were revealed by Hu immunoreactivity. Dorsal views are shown. Scale bar: 25 μm. (**B**) At 72 hpf, there were 40-fold more RB cells in 1.6MO morphants (n=12) versus control (n=9) embryos (*$P \leqslant 0.003$).

Injection of 1.6MO prolonged survival of RB cells

A consequence of reduced Na^+ current in RB cells is an increase in survival rather than loss by normal programmed cell death (Svoboda et al., 2001). As a result of the diminished Na^+ current amplitudes in RB cells of morphants (Fig. 3F,G), we predicted that RB cells would survive longer in morphant versus control embryos. At 72 hpf, examination of RB cell bodies revealed that injection of 1.6, but not control, MO led to an increase in RB survival (Fig. 4), as expected because of the loss of Na^+ current (Fig. 4) (Svoboda et al., 2001).

Axonal trajectories of motor neurons were abnormal in 1.6MO morphants embryos

In addition to RB cells, specific populations of motoneurons expressed *scn8a*. CaPs and dorsally projecting SMNs expressed the gene (Figs 1, 2). Recent studies provided evidence that perturbation of activity in all embryonic spinal neurons during stages of neurite outgrowth altered neurotransmitter expression (Borodinsky et al., 2004). However, the extent to which activity regulates the development of motoneurons is poorly understood. The restricted pattern of *scn8a* expression in select motoneuron populations allowed us to examine the role of activity in development of specific zebrafish motoneurons.

We examined morphological development of motoneurons using znp-1 and SV-2, antibodies that recognize proteins present in both PMNs and SMNs (Fig. 5). In addition, we assessed target recognition by comparing the location of antibody labeling to that of postsynaptic receptors detected by α-bungarotoxin. At 48 hpf, little difference was noted between ventrally projecting axons of 1.6MO morphants versus control injected embryos (Fig. 5A,B). However, by 72 hpf, morphologies of motoneuron axons differed in 1.6MO morphants versus controls (Fig. 5C,D). In morphant embryos, axons branched more. Moreover, in controls, the most distally labeled region of motoneuron axons typically were aligned with postsynaptic receptors by 72 hpf (Fig. 5C) (LeFebvre et al., 2004; Panzer et al., 2005). By contrast, in morphants, the distal processes of several motoneuron axons did not align with postsynaptic receptors (Fig. 5D). Analysis of the SV-2 and α-bungarotoxin signals in the distal regions of axons of control and morphant embryos indicated 84 versus 71% colocalization at 72 hpf (n=9 and 11, respectively; P<0.0004). Thus, the results indicated that 1.6MO injection altered morphological development of motoneuron axons and their contacts with muscle cells.

After ~28 hpf, both PMN and SMN axons contribute to the ventral projections but SV-2 and znp-1 antibodies recognize both types of axons (Pike et al., 1992; Ott et al., 2001). Thus, SMN, PMN, or both types of axons, could be defective. Because CaPs but not ventrally projecting SMNs expressed *scn8a* (Figs 1, 2), we expected that the defects in motoneuron axonal trajectories detected by SV-2 or znp-1 were consequent to effects of 1.6MO on CaP axons. Furthermore, because PMN axons serve as pioneers and establish a scaffold for SMN outgrowth (for a review, see Lewis and Eisen, 2003), abnormal CaP axons would induce aberrant morphology of SMN axons (Pike et al., 1992).

To test whether CaP axons were affected by injection of the 1.6 MO, we examined their ventral projections. At 21-24 hpf, the patterns of znp-1 immunoreactivity did not differ between 1.6 and control morphant embryos (Fig. 5E-H). Furthermore, individually dye-labeled CaP axons did not differ between 1.6 and control morphant embryos (Fig. 5I,J). Moreover, morphological aspects of synapse formation also appeared to be similar on the basis of the relative positions of SV-2 and α-bungarotoxin signals (Fig. 5K,L). Thus, no defects were noted in CaP axon morphology as a result of the 1.6MO injection, implicating SMN axons in the defective ventral projections present in 1.6MO morphants.

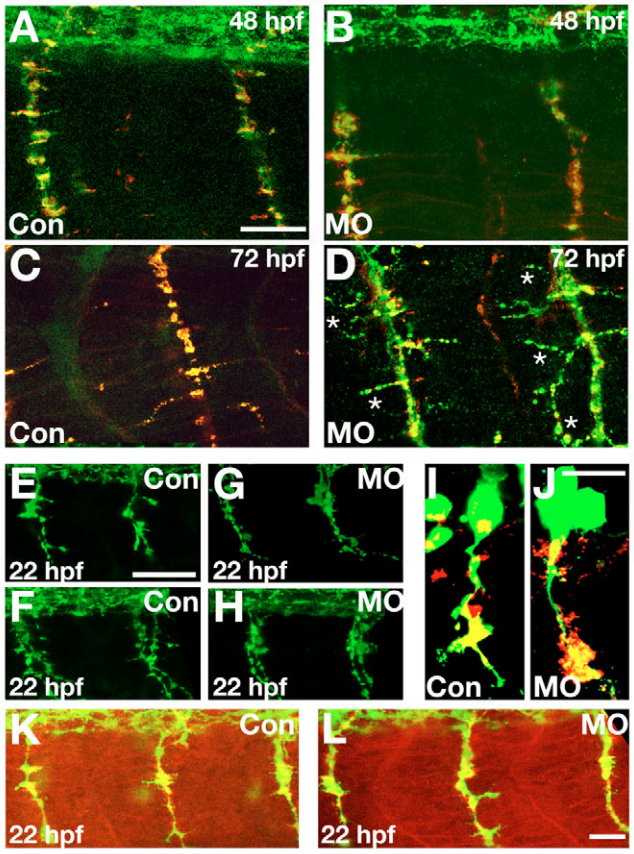

Fig. 5. Ventrally projecting motor axons displayed abnormal trajectories in 1.6MO morphants even though CaP axons project normally. (**A-D**) Motor axon morphology was assayed using SV-2 immunoreactivity (green) in conjunction with a marker of the muscle postsynaptic receptor, α-bungarotoxin (red). At 48 hpf (A,B), little difference was noted in znp-1 immunoreactivity of motor axons of 1.6MO morphants (B) compared with control-injected embryos (A). However, by 72 hpf, there were marked differences (C,D). Motor axons of 1.6MO morphants (D, asterisks) branched more than those of control-injected embryos. Moreover, in morphants (D), there was a reduction in the normal alignment between motor axons and postsynaptic receptors, assessed by the near absence of green and abundance of yellow in C versus the reduction in yellow and increase in green in panel D. (**E-L**) Injection of 1.6MO did not affect axon outgrowth from CaP when synapses first form. (E-H) At 21-22 hpf, znp-1 immunoreactivity revealed no differences between ventrally projecting CaP axons in either control (E,F) or 1.6MO-injected (G,H) embryos. Embryos were squash-mounted and, consequently, motor nerves on both sides of an embryo were often present in a single confocal section (e.g. F,H). (I,J) CaPs were directly labeled by dye injection (green) at 20 hpf and embryos were fixed at 21-22 hpf and stained for SV-2 immunoreactivity. Injection of either ConMO (I) or 1.6MO (J) did not affect CaP axon morphology. (K,L) In addition to axonal morphology (SV-2, green), postsynaptic specializations, as detected by α-bungarotoxin labeling (red) were not altered by injection of either Con (K) or 1.6 (L) MO. Scale bars: in A, 20 μm for A,B; 30 μm for C; in E, 50 μm for E-H; in J, 10 μm for I,J; in L, 20 μm for K,L.

Axonal trajectories of secondary motor neurons were abnormal in 1.6MO morphant embryos

We next tested directly whether SMN axons were affected by 1.6MO injection by using the zn-8 antibody that recognizes neurolin (DM-GRASP), a cell-surface protein expressed by SMNs but not PMNs (Fig. 6) (Fashena and Westerfield, 1999; Ott et al., 2001). Beginning at ~30 hpf, neurolin is initially detected in both the cell bodies and emerging axons of SMNs (Fig. 6A). By 72 hpf, cell body expression is downregulated but axonal labeling persists (Fig. 6E) (Ott et al., 2001). Typically, at the choice point near the horizontal myoseptum, the motor nerve forms three distinct branches by 66 hpf (Fig. 6C) (Fashena and Westerfield, 1999; Ott et al., 2001). One branch contains axons of dorsally projecting SMNs. (Fig. 6C, arrowheads). The second branch contains axons of ventrally projecting SMNs (Fig. 6C, asterisks). A third branch projects rostrally within the vicinity of the horizontal myoseptum (Fig. 6C, arrows).

At 48 hpf, little difference was observed in zn-8 immunoreactivity between 1.6MO- and control-injected embryos (Fig. 6A versus B). However, at this stage only the common branch of all axons to the myoseptum choice point was present. At 66 hpf (Fig. 6C,D), 1.6MO morphants consistently lacked the rostrally projecting nerves that were now present in controls (arrows). In addition, SMN axons that projected dorsally were not detected by zn-8 at 66 hpf in 1.6MO morphants although they were present in all segments of controls (Fig. 6C versus D; arrowheads). At 78 hpf, rostral branches were still absent in some segments in 1.6MO morphants (Fig. 6F, arrows). In addition, some dorsal segments still lacked dorsally projecting SMN axons (Fig. 6F, arrowhead). We followed recovery of innervation of the dorsal musculature to later times (Fig. 6G). By 144 hpf, recovery of dorsal muscle innervation was still not complete. The time course of recovery is consistent with that expected for turnover of MOs (Nasevicius and Ekker, 2000) (see Discussion).

As recovery of rostral and dorsal SMN motor nerves occurred, the axons of ventrally projecting SMNs began to display abnormal properties (Table 2). In 88% (21/24) of 1.6MO morphants, more than one ventrally projecting nerve was present in at least one segment of the embryo (Fig. 6H). Such additional ventral roots were not observed in control embryos. In addition, the distal ends of ventrally projecting SMN axons branched more and appeared more splayed than did those in control injected embryos (Fig. 6I,J, asterisks; Table 2). This phenotype was not observed in control injected embryos (0/32) but was present in 54% (13/24) of 1.6MO morphant embryos. Interestingly, in the three 1.6MO morphants embryos that did not display an additional ventral root, the branching phenotype was present. Thus, all 1.6MO morphants displayed at least one of two different ventral phenotypes.

The phenotype detected in ventrally projecting SMN axons was surprising for two reasons. First, the phenotype was not apparent until 72 hpf and worsened subsequently – a time course that is hard to reconcile with MO turnover. Second, *scn8a* was not detected in ventrally projecting SMNs (Fig. 2). Consequently, we were concerned that the 1.6MO might have produced a non-specific but general effect on axon outgrowth in the trunk. To test this possibility, we examined the morphology of reticulospinal Mauthner cells and their axons using the 3A10 antibody (Hatta, 1992). Mauthner cell axons project caudally in the spinal cord in the vicinity of motoneuron cell bodies and initial axon segments (Kimmel et al., 1982) but do not express *scn8a* (Novak et al., 2006a). Mauthner neurons of 1.6MO morphants appeared normal (Fig. 6K-N). Their somata were normal in shape and size, and their contralaterally projecting axons displayed normal trajectories. At 72 hpf, a time

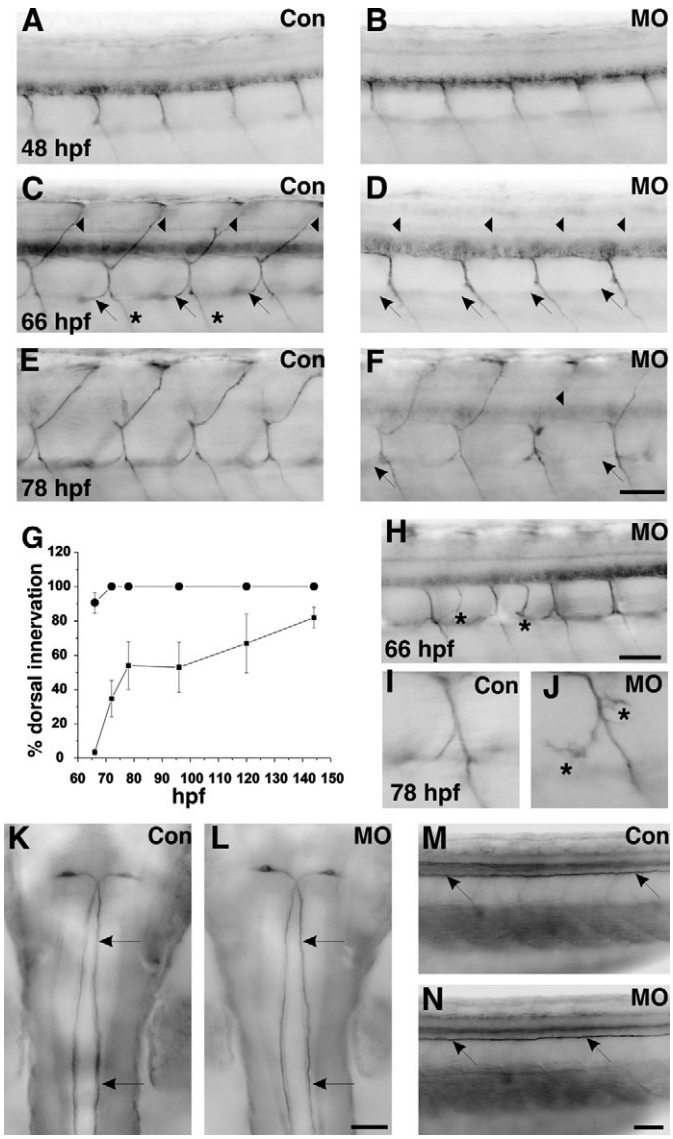

Fig. 6. Injection of 1.6MO altered SMN axons although Mauthner axons projected normally. (**A-F**) Zn-8 immunoreactivity revealed differences in SMN axon outgrowth between morphants and controls. Between 48 and 66 hpf (A-D), innervation of the dorsal musculature was reduced in 1.6MO morphants (B,D) versus control (A,C). Arrows and arrowheads in C,D,F indicate the rostral and dorsal projections. Asterisks in C indicate ventral projections. At 78 hpf (E,F), substantial recovery had occurred in 1.6MO morphants (F) and the majority of dorsal somites were innervated. (**G**) Although 1.6MO morphants (squares) initially displayed no innervation of the dorsal musculature, this phenotype recovered. Recovery began at 3 dpf and was nearly complete by 5 dpf. Circles represent data from control embryos. (**H**) In ventral muscle at 66 hpf, extra ventrally projecting axons (asterisks) were present in 28.8±3.6% of segments in 1.6MO morphants but were not present in controls. (**I**,**J**) At 78 hpf, the axons of ventrally projecting SMNs in 1.6MO morphants branched more (J) compared with controls (I), consistent with results obtained with the znp-1 antibody (cf. Fig. 5C,D). (**K-N**) Injection of 1.6MO did not affect Mauthner cell axonal morphology. (K,L) Mauthner cell axons projected caudally into spinal cord in 48 hpf 1.6MO morphants (L) and controls (K). (M,N) Mauthner axons of 72 hpf 1.6MO morphants (N) displayed morphologies similar to those of controls (M). Scale bars: in F, 40 μm for A-F; in H, 40 μm for H and 20 μm for I,J; in L 40 μm for K,L; in N, 40 μm for M,N.

Table 2. Prevalence of ventrally projecting SMN phenotypes

Group (n)	Excess branching		Extra ventral nerve	
	Embryos	Segments/embryo	Embryos	Segments/embryo
Morphant (24)	88%*	28.8±3.6%†	54%‡	11.7±2.5%§
Control (32)	0%	0±0 %	0%	0±0%

Embryos indicate the percentage of embryos that displayed the phenotype.
Segments/embryo indicates the percent of segments examined per embryo that displayed the phenotype.
Analysis was restricted to approximately six segments dorsal to the yolk sac extension. Statistical comparisons between morphant and control groups were carried out using either a two-sided Fisher's exact test (*,†) or a *t*-test assuming unequal variances (‡,§).
*$P<1.5\times10^{-12}$; †$P<1.3\times10^{-6}$; ‡$P<4\times10^{-8}$; §$P<1\times10^{-4}$.

when defects in SMN axons were detected in 1.6MO morphants, Mauthner cells axons had normal trajectories within the spinal cord (Fig. 6M,N). These results indicated that the 1.6MO did not have a non-specific general effect on axonal growth in the spinal cord.

Another possibility that we considered is that 1.6MO injection altered expression of neurolin, as detected by zn-8 labeling, but did not perturb axonal outgrowth directly. Typically, neurolin is downregulated in SMN cell bodies by 72 hpf. However, in 1.6MO morphants, neurolin persisted in SMN cell bodies at 72 hpf, supporting this possibility (Fig. 6F). To avoid this potential problem, we examined axonal trajectories in the Tg(gata2:GFP) line (Fig. 7). In Tg(gata2:GFP)-treated embryos, GFP+ ventrally projecting SMN axons (Fig. 7B,D,E) displayed phenotypes similar to those detected by zn-8 immunocytochemistry (Fig. 6). Specifically, GFP+ axons branched much more extensively in morphant embryos (Fig. 7B,D,E) than they did in controls (Fig. 7A,C). These results indicate that, despite the lack of detection of *scn8a* in ventrally projecting SMNs, their axonal trajectories were perturbed by injection of 1.6MO.

Mosaic analysis reveals cell non-autonomous effect of 1.6MO on ventrally projecting SMNs

The results presented above suggest that $Na_v1.6a$ channels exert non-autonomous effects on axons of ventrally projecting SMNs. If so, ventrally projecting SMNs would develop normally if they did contain the 1.6MO but other cells did not. Conversely, ventrally projecting SMNs would show defects if they did not contain the 1.6MO but other cells did. To test directly for non-cell autonomous effects of $Na_v1.6a$, we performed mosaic analysis by injecting single cells of 2-3 hpf embryos with 1.6MO and lineage tracer (Fig. 8).

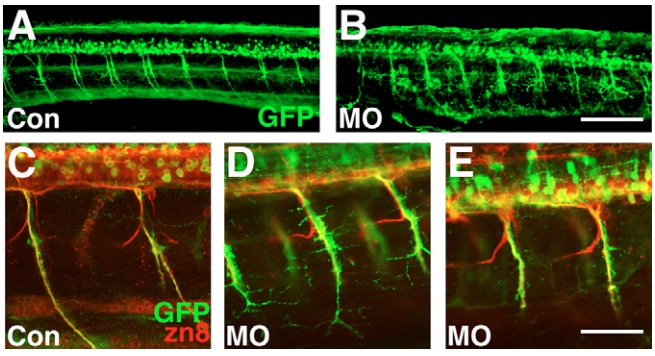

Fig. 7. Injection of 1.6MO but not ConMO perturbed outgrowth of SMN axons in Tg(gata2:GFP) embryos. (**A-E**) GFP+ ventrally projecting axons displayed more branching in Tg(gata2:GFP) morphant (B,D,E) but not control (A,C) embryos at 72 hpf. Embryos were squash-mounted and, consequently, motor nerves on both sides of an embryo were often present in a single confocal section (e.g. A,B). Scale bars: in B, 100 μm for A,B; in E, 50 μm for C-E.

Consistent with our predictions, when the 1.6MO was present in ventrally projecting SMNs, their axons developed normally in all cases (*n*=6/6; Fig. 8B). Conversely, when the 1.6MO was present in other spinal cord neurons but absent from ventrally projecting neurons, SMN axons showed defects in 44% of embryos (*n*=10/23) similar to when the 1.6MO was present throughout the embryo (e.g. Fig. 7). Even though the effects on axons of ventrally projecting SMNs were stronger when the 1.6MO was present throughout the

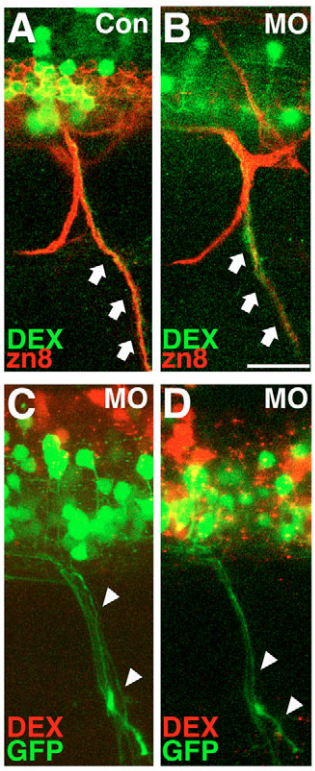

Fig. 8. Effects of the 1.6MO on ventrally projecting SMN axons are non cell-autonomous. In wild-type embryo mosaics (**A**,**B**), the presence of the 1.6MO (B) or ConMO (A) in ventrally projecting SMNs did not produce abnormally projecting axons. The lineage tracer fluorescein-conjugated dextran (green) was co-injected with the MO. SMN axons were revealed by zn8 immunocytochemistry (red). Ventrally projecting axons (arrows) are both zn8+ (red) and GFP+ (green), indicating that they contain axons of neurons derived from the MO-injected cell. (**C**,**D**) In embryos of the Tg(gata2:GFP) line, GFP+ (green) axons were abnormal even though they did not contain the lineage tracer rhodamine-conjugated dextran (red). However, other spinal neurons were positive for the lineage tracer (red), indicating that the 1.6MO had non cell-autonomous effects of ventrally projecting SMNs. Each panel contains a projection of six consecutive confocal sections. Scale bar: 40 μm.

embryo, the presence of the 1.6MO in just a few other spinal cord neurons was sufficient to produce aberrant morphology of ventrally projecting SMN axons (Fig. 8C,D). The ConMO had no effects, regardless of its location (n=13/13). Overall, the results of mosaic analyses revealed that ventrally projecting SMNs required $Na_v1.6a$ non cell-autonomously in order to develop normal axonal morphologies.

DISCUSSION

Although it is well known that activity-dependent cues guide neuronal development, little is known about the specific contributions of voltage-gated Na^+ channels to these mechanisms. Here, we show that knockdown of the $Na_v1.6a$ channel in the zebrafish embryo led to morphological defects in axons of specific spinal motoneuron subtypes. Moreover, the results revealed that $Na_v1.6a$ knockdown had both cell-autonomous as well as non cell-autonomous effects on motoneuron axons.

Voltage-gated Na^+ channels reside in the plasma membrane and provide an entry point for extracellular Na^+ to the neuronal cytoplasm. Their functional elimination would be expected to result in cell-autonomous effects. Consistent with this, RB Na^+ current amplitude and cell death were reduced (Figs 3, 4), and dorsally projecting SMNs displayed a significant delay in axon outgrowth in morphant embryos (Fig. 6). The latter phenotype recovered with a time course expected for MO turnover (Nasevicius and Ekker, 2000), suggesting that blockade of $Na_v1.6a$ translation prior to 72 hpf prevented axon outgrowth from these SMNs; later, when MO concentrations fell, translation of $Na_v1.6a$ began, allowing recovery of axon outgrowth.

Some neurons that express *scn8a* did not display a phenotype. Notably, CaPs expressed *scn8a* but developed normal axonal trajectories when $Na_v1.6a$ was knocked down (Fig. 5). Interestingly, CaP axons also developed normally in *nic1*^{b107} mutants, that are immotile as a result of a null-type mutation in the α-subunit of the postsynaptic muscle acetylcholine receptor (Liu and Westerfield, 1990; Westerfield et al., 1990; Sepich et al., 1998). By contrast, a different mutation in the muscle acetylcholine receptor α-subunit gene (*twister*; *nic1*$^{twister\ dbn12}$), results in excessive activity and *twister* mutants move in an uncoordinated manner (Lefebvre et al., 2004). Furthermore, unlike *nic1*^{b107} mutants, *twister* mutants display abnormal PMN axonal trajectories and muscle degeneration (Lefebvre et al., 2004). Thus, blockade of the muscle postsynaptic receptor has no effect on CaP axons, whereas hyperactivity results in defective CaP axons.

Surprisingly, $Na_v1.6a$ knockdown led to abnormal axon outgrowth in an unexpected motoneuron subtype, the ventrally projecting SMN, that did not display *scn8a* expression (Fig. 2). Both immunocytochemical staining (zn-8) as well as direct GFP labeling [Tg(gata2:GFP)] revealed abnormal axonal morphologies, eliminating the possibility that the phenotype resulted from abnormal expression of neurolin (Figs 6, 7). CaP axons were also normal (Fig. 5), ruling out abnormal pioneer axon morphology as a basis for the defective SMN axonal trajectories. These results implicated Na^+ channels unexpectedly in non-cell-autonomous as well as cell-autonomous developmental roles, a conclusion that was further supported by mosaic analyses.

With respect to the mosaic analyses, one potential caveat is that although morpholino knockdown significantly reduces $Na_v1.6a$ protein levels, it might not entirely eliminate it. If this were the case and if reduced levels of $Na_v1.6a$ sufficed to achieve its function in ventrally projecting SMNs, our mosaic experiments might incorrectly suggest that $Na_v1.6a$ did not cell-autonomously affect this cell type (e.g. Fig. 8B). However, the mRNA encoding $Na_v1.6a$, *scn8a*, was not detected in ventrally projecting SMNs even though it was present in dorsally projecting SMNs (Fig. 2), suggesting that 1.6MOs had no effect on ventrally projecting SMNs because these neurons did not express the targeted gene. Moreover, morpholino knockdown of $Na_v1.6a$ protein in cells other than ventrally projecting SMNs sufficed to reveal non cell-autonomous effects (Fig. 8C,D).

Previous studies revealed that absence of PMNs had complex effects on SMNs that differed depending on whether SMNs projected axons dorsally or ventrally (Pike et al., 1992). The results suggested that the axons of different SMN subtypes have distinct abilities to recognize guidance cues (Pike et al., 1992). Our present results are consistent with this idea. Pike et al. (Pike et al., 1992) proposed that cues on PMN axons are directly responsible for some aspects of SMN axon guidance. In light of recent studies demonstrating the importance of developmentally regulated modification of the substrata on which motor axons navigate (Zhang et al., 2004; Schneider and Granato, 2006), another possible interpretation is that in the absence of $Na_v1.6a$, even though CaP axons extend normally, they fail to interact correctly with their environment; consequently, the environment is altered so that SMN axons cannot extend properly, or interactions between the CaP and SMN somata are altered, resulting in failure of the SMNs to extend axons properly. These possibilities can be addressed in future experiments.

Even though morpholinos have been used with great success in zebrafish, not all morpholinos work as expected, requiring control experiments such as rescue by RNA overexpression, reduction of targeted protein levels or function, use of appropriate control morpholinos and/or RT-PCR analysis of mRNA when using splice-blocking morpholinos (Nasevicius and Ekker, 2000). Rescue experiments typically involve injection of the targeted RNA immediately after injection of the MO. However, *scn8a* RNA overexpression by itself produced phenotypes similar to those produced by 1.6MO injection (e.g. reduced touch sensitivity). In these experiments, the injected *scn8a* RNA is expected to be present in cells that normally express the gene, as well as in cells that do not, and ectopic expression of *scn8a* might have resulted in abnormal function of the relevant circuits. Moreover, rescue by *scn8a* injection was complicated by the fact that injection of both 1.6MO and *scn8a* mRNA resulted in profound embryonic lethality, with few surviving severely deformed embryos. These effects of *scn8a* overexpression either alone or in combination with 1.6MO prevented interpretation of *scn8a* rescue experiments.

Several other standard control experiments were successful. For each 1.6MO, we compared results to those obtained with a specific control morpholino that differed from a 1.6MO by four or five base mismatches (see Materials and methods). We used three different translation-blocking MOs that had dose-dependent effects (Pineda et al., 2005). In addition to the three different translation blocking morpholinos, we also used a splice-blocking morpholino along with its own specific control morpholino. The splice-blocking morpholino, but not its control, resulted in incorrect processing of *scn8a* mRNA, even at 72 hpf (Fig. 3A). 1.6MO injection resulted in reduced Na^+ channel levels, detected either immunocytochemically (Fig. 3B-E) or electrophysiologically (Fig. 3F,G). Moreover, 1.6MOs mimicked a previously reported effect of reduced Na^+ channel function – reduction of RB cell apoptosis (Fig. 4) (Svoboda et al., 2001). In summary, several lines of evidence support the conclusion that the 1.6MO effects resulted from $Na_v1.6a$ knockdown.

The small number and earlier development of PMNs versus SMNs (Beattie et al., 1997) has facilitated studies of PMN axon guidance mechanisms. Despite the limited data regarding SMNs, it is clear that PMNs and SMNs share some aspects of axon guidance mechanisms because both rely upon myotomal derived signals (Zeller et al., 2002). In addition, a few studies have provided evidence for SMN-specific axon growth/guidance mechanisms. For example, neurolin is required for normal development of SMN but not PMN axons (Ott et al., 2001). Further, nicotine exposure affects morphology of SMN axons (Svoboda et al., 2002). However, nicotine exposure began at 22 hpf, well after initiation of, and possibly too late for, effects on PMN axon outgrowth. A recently isolated mutant, *where's waldo* (*wdo*), displays defects in SMN axon outgrowth, and many segments lack the SMN component of the dorsal nerve similar to 1.6MO morphants (Panzer et al., 2005) (this study). In light of our findings, the effects of muscle inactivity (*nic1*^{b107}) and hyperactivity (*twister*) on SMN axon morphology both warrant examination.

The mammalian gene *Scn8a* is orthologous to *scn8a* (Novak et al., 2006b). The mouse mutant *med* lacks a functional *Scn8a* gene and displays aberrant sprouting of motor nerve terminals similar to the highly branched axons of ventrally projecting SMNs of 1.6MO morphants (Figs 5, 7) (Duchen, 1970; Burgess et al., 1995). *med* mutants also show neonatal hindlimb paralysis (Duchen, 1970). Similarly, 1.6MO morphants became severely immotile at 5 dpf, suggesting a progressive or delayed deterioration of the neuromuscular system. Although the defects that we report here would be expected to reduce motility of 1.6MO morphants, it is not clear why 1.6MO morphants developed such extensive paralysis, especially at stages after extensive MO turnover. If there were early crucial periods for the developmental roles of $Na_v1.6a$, not all phenotypes would recover, perhaps leading to degeneration of neuromuscular junctions. In addition, larvae use PMNs primarily for escape responses and SMNs primarily for swimming (Liu and Westerfield, 1990). Because ventrally projecting SMNs are affected in 1.6MO morphants, the entire ventral musculature may not contract sufficiently to allow normal swimming. Further studies of 3 dpf or older larvae are needed to resolve this issue.

In summary, our data indicate that knockdown of a specific Na^+ channel isotype affects SMN axon outgrowth. The effects of $Na_v1.6a$ knockdown on SMN axon outgrowth occur in cells that express *scn8a* (e.g. dorsally projecting SMNs) as well as those that do not (e.g. ventrally projecting SMNs), indicating both cell autonomous and non-autonomous effects of a voltage-gated Na^+ channel on axonal development. It is not yet known how $Na_v1.6a$-dependent effects are spread to neurons that do not express the *scn8a* gene. The underlying mechanisms might involve altered secretion of neuronal neurotrophic or muscle retrograde factors (see above) and/or the extensive electrical coupling that is present in the embryonic spinal cord (Saint-Amant and Drapeau, 2000; Saint-Amant and Drapeau, 2001). Overall, the results demonstrate that voltage-gated neuronal Na^+ channels play developmental and conventional excitability roles in the vertebrate nervous system.

We thank Ryan Heiser, Daryl Weldon and Sarah Stroh for fish care; Dr A. Douglas Robertson for help with statistical analysis; Dr John Caldwell and members of the Ribera laboratory for comments on the manuscript. Supported by NIH grants NS23915 (JSE), and NS038937 & NS048154 (ABR).

References

Appel, B., Korzh, V., Glasgow, E., Thor, S., Edlund, T., Dawid, I. B. and Eisen, J. S. (1995). Motoneuron fate specification revealed by patterned LIM homeobox gene expression in embryonic zebrafish. *Development* **121**, 4117-4125.

Beattie, C. E., Hatta, K., Halpern, M. E., Liu, H., Eisen, J. S. and Kimmel, C. B. (1997). Temporal separation in the specification of primary and secondary motoneurons in zebrafish. *Dev. Biol.* **187**, 171-182.

Borodinsky, L. N., Root, C. M., Cronin, J. A., Sann, S. B., Gu, X. and Spitzer, N. C. (2004). Activity-dependent homeostatic specification of transmitter expression in embryonic neurons. *Nature* **429**, 523-530.

Burgess, D. L., Kohrman, D. C., Galt, J., Plummer, N. W., Jones, J. M., Spear, B. and Meisler, M. H. (1995). Mutation of a new sodium channel gene, Scn8a, in the mouse mutant 'motor endplate disease'. *Nat. Genet.* **10**, 461-465.

Duchen, L. W. (1970). Hereditary motor end-plate disease in the mouse: light and electron microscopic studies. *J. Neurol. Neurosurg. Psychiatr.* **33**, 238-250.

Duchen, L. W. and Stefani, E. (1971). Electrophysiological studies of neuromuscular transmission in hereditary 'motor end-plate disease' of the mouse. *J. Physiol.* **212**, 535-548.

Eisen, J. S. (1992). The role of interactions in determining cell fate of two identified motoneurons in the embryonic zebrafish. *Neuron* **8**, 231-240.

Eisen, J. S. and Melancon, E. (2001). Interactions with identified muscle cells break motoneuron equivalence in embryonic zebrafish. *Nat. Neurosci.* **4**, 1065-1070.

Eisen, J. S., Myers, P. and Westerfield, M. (1986). Pathway selection by growth cones of identified motoneurones in live zebrafish embryos. *Nature* **320**, 269-271.

Fashena, D. and Westerfield, M. (1999). Secondary motoneuron axons localize DM-GRASP on their fasciculated segments. *J. Comp. Neurol.* **406**, 415-424.

Gamse, J. T., Thisse, C., Thisse, B. and Halpern, M. E. (2003). The parapineal mediates left-right asymmetry in the zebrafish diencephalon. *Development* **130**, 1059-1068.

Gu, X. and Spitzer, N. C. (1995). Distinct aspects of neuronal differentiation encoded by frequency of spontaneous Ca^{2+} transients. *Nature* **375**, 784-787.

Hanson, M. W. and Landmesser, L. T. (2004). Normal patterns of spontaneous activity are required for correct motor axon guidance and the expression of specific guidance molecules. *Neuron* **43**, 687-701.

Harada, A., Takeuchi, K., Dohmae, N., Takio, K., Uenaka, T., Aoki, J., Inoue, K. and Umeda, M. (1999). A monoclonal antibody, 3A10, recognizes a specific amino acid sequence present on a series of developmentally expressed brain proteins. *J. Biochem.* **125**, 443-448.

Hatta, K. (1992). Role of floor plate in axonal patterning in the zebrafish CNS. *Neuron* **9**, 629-642.

Henion, P. D., Raible, D. W., Beattie, C. E., Stoesser, K. L., Weston, J. A. and Eisen, J. S. (1996). Screen for mutations affecting development of Zebrafish neural crest. *Dev. Genet.* **18**, 11-17.

Higashijima, S., Hotta, Y. and Okamoto, H. (2000). Visualization of cranial motor neurons in live transgenic zebrafish expressing green fluorescent protein under the control of the islet-1 promoter/enhancer. *J. Neurosci.* **20**, 206-218.

Inoue, A., Takahashi, M., Hatta, K., Hatta, Y. and Okamoto, H. (1994). Developmental regulation of islet-1 mRNA expression during neuronal differentiation in embryonic zebrafish. *Dev. Dyn.* **199**, 1-11.

Kimmel, C. B., Powell, S. L. and Metcalfe, W. K. (1982). Brain neurons which project to the spinal cord in young larvae of the zebrafish. *J. Comp. Neurol.* **205**, 112-127.

Kimmel, C. B., Ballard, W. W., Kimmel, S. R., Ullmann, B. and Schilling, T. F. (1995). Stages of embryonic development of the zebrafish. *Dev. Dyn.* **203**, 253-310.

Lefebvre, J. L., Ono, F., Puglielli, C., Seidner, G., Franzini-Armstrong, C., Brehm, P. and Granato, M. (2004). Increased neuromuscular activity causes axonal defects and muscular degeneration. *Development* **131**, 2605-2618.

Lewis, K. E. and Eisen, J. S. (2003). From cells to circuits: development of the zebrafish spinal cord. *Prog. Neurobiol.* **69**, 419-449.

Liu, D. W. and Westerfield, M. (1988). Function of identified motoneurones and co-ordination of primary and secondary motor systems during zebra fish swimming. *J. Physiol.* **403**, 73-89.

Liu, D. W. C. and Westerfield, M. (1990). The formation of terminal fields in the absence of competitive interactions among primary motoneurons in the zebrafish. *J. Neurosci.* **10**, 3947-3959.

Marusich, M. F., Furneaux, H. M., Henion, P. D. and Weston, J. D. (1994). Hu neuronal proteins are expressed in proliferating neurogenic cells. *J. Neurobiol.* **25**, 143-155.

Meng, A., Tang, H., Ong, B. A., Farrell, M. J. and Lin, S. (1997). Promoter analysis in living zebrafish embryos identifies a cis-acting motif required for neuronal expression of GATA-2. *Proc. Natl. Acad. Sci. USA* **94**, 6267-6272.

Metcalfe, W. K., Myers, P. Z., Trevarrow, B., Bass, M. B. and Kimmel, C. B. (1990). Primary neurons that express the L2/HNK-1 carbohydrate in the zebrafish. *Development* **110**, 491-504.

Ming, G., Henley, J., Tessier-Lavigne, M., Song, H. and Poo, M.-M. (2001). Electrical activity modulates growth cone guidance by diffusible factors. *Neuron* **29**, 441-452.

Nasevicius, A. and Ekker, S. C. (2000). Effective targeted gene 'knockdown' in zebrafish. *Nat. Genet.* **26**, 216-220.

Novak, A. E. and Ribera, A. B. (2003). Immunocytochemistry as a tool for zebrafish developmental neurobiology. *Methods Cell Sci.* **25**, 79-83.

Novak, A. E., Taylor, A. D., Pineda, R. H., Lasda, E. L., Wright, M. A. and Ribera, A. B. (2006a). Embryonic and larval expression of zebrafish voltage-gated sodium channel alpha-subunit genes. *Dev. Dyn.* **235**, 1962-1973.
Novak, A. E., Jost, M. C., Lu, Y., Taylor, A. D., Zakon, H. H. and Ribera, A. B. (2006b). Gene duplications and evolution of vertebrate voltage-gated sodium channels. *J. Mol. Evol.* **63**, 208-221.
Ott, H., Diekmann, H., Stuermer, C. A. O. and Bastmeyer, M. (2001). Function of neurolin (DM-GRASP/SC-1) in guidance of motor axons during zebrafish development. *Dev. Biol.* **235**, 86-97.
Panzer, J. A., Gibbs, S. M., Dosch, R., Wagner, D., Mullins, M. C., Granato, M. and Balice-Gordon, R. J. (2005). Neuromuscular synaptogenesis in wild-type and mutant zebrafish. *Dev. Biol.* **285**, 340-357.
Pike, S. H., Melancon, E. and Eisen, J. S. (1992). Pathfinding by zebrafish motoneurons in the absence of normal pioneer axons. *Development* **114**, 825-831.
Pineda, R. H., Heiser, R. A. and Ribera, A. B. (2005). Molecular determinants of I_{Na} *in vivo* in embryonic zebrafish sensory neurons. *J. Neurophysiol*. **93**, 3582-3593.
Ribera, A. B. and Nüsslein-Volhard, C. (1998). Zebrafish touch-insensitive mutants reveal an essential role for the developmental regulation of sodium current. *J. Neurosci.* **18**, 9181-9191.
Saint-Amant, L. and Drapeau, P. (2000). Motoneuron activity patterns related to the earliest behavior of the zebrafish embryo. *J. Neurosci.* **20**, 3964-3972.
Saint-Amant, L. and Drapeau, P. (2001). Synchronization of an embryonic network of identified spinal interneurons solely by electrical coupling. *Neuron* **31**, 1035-1046.
Sanes, J. R. and Lichtman, J. W. (2001). Induction, assembly, maturation and maintenance of a postsynaptic apparatus. *Nat. Rev.* **2**, 791-805.
Schneider, V. A. and Granato, M. (2003). Motor axon migration: a long way to go. *Dev. Biol.* **263**, 1-11.
Schneider, V. A. and Granato, M. (2006). The myotomal diwanka (lh3) glycosyltransferase and type XVIII collagen are critical for motor growth cone migration. *Neuron* **50**, 683-695**.**
Sepich, D. S., Wegner, J., O'Shea, S. and Westerfield, M. (1998). An altered intron inhibits synthesis of the acetylcholine receptor alpha-subunit in the paralyzed zebrafish mutant nic1. *Genetics* **148**, 361-372.
Spitzer, N. C., Root, C. M. and Borodinsky, L. N. (2004). Orchestrating neuronal differentiation: patterns of Ca^{2+} spikes specify transmitter choice. *Trends Neurosci.* **27**, 415-421.
Svoboda, K. R., Linares, A. E. and Ribera, A. B. (2001). Activity regulates programmed cell death of zebrafish Rohon-Beard neurons. *Development* **128**, 3511-3520.
Svoboda, K. R., Vijayaraghavan, S. and Tanguay, R. L. (2002). Nicotinic receptors mediate changes in spinal motoneuron development and axonal pathfinding in embryonic zebrafish exposed to nicotine. *J. Neurosci.* **22**, 10731-10741.
Tokumoto, M., Gong, Z., Tsubokawa, T., Hew, C. L., Uyemura, K., Hotta, Y. and Okamoto, H. (1995). Molecular heterogeneity among primary motoneurons and within myotomes revealed by the differential mRNA expression of novel islet-1 homologs in embryonic zebrafish. *Dev. Biol.* **171**, 578-589.
Trevarrow, B., Marks, D. L. and Kimmel, C. B. (1990). Organization of hindbrain segments in the zebrafish embryo. *Neuron* ***4***, 669-679.
Tsai, C. W., Tseng, J. J., Lin, S. C., Chang, C. Y., Wu, J. L., Hong, J. F. and Tsay, H. J. (2001). Primary structure and developmental expression of zebrafish sodium channel Na(v)1.6 during neurogenesis. *DNA Cell Biol.* **20**, 249-255.
Watt, S. D., Gu, X., Smith, R. D. and Spitzer, N. C. (2000). Specific frequencies of spontaneous Ca^{2+} transients upregulate GAD 67 transcripts in embryonic spinal neurons. *Mol. Cell Neurosci.* ***16***, 376-387.
Westerfield, M. (1995). *The Zebrafish Book*. Eugene: The University of Oregon Press.
Westerfield, M., Liu, D. W., Kimmel, C. B. and Walker, C. (1990). Pathfinding and synapse formation in a zebrafish mutant lacking functional acetylcholine receptors. *Neuron* **4**, 867-874.
Zeller, J., Schneider, V., Malayaman, S., Higashijima, S., Okamoto, H., Gui, J., Lin, S. and Granato, M. (2002). Migration of zebrafish spinal motor nerves into the periphery requires multiple myotome-derived cues. *Dev. Biol.* **252**, 241-256.
Zhang, J., Lefebvre, J. L., Zhao, S. and Granato, M. (2004). Zebrafish unplugged reveals a role for muscle-specific kinase homologs in axonal pathway choice. *Nat. Neurosci.* **7**, 1303-1309.